Influence of the N atom position on the excited state photodynamics of protonated azaindole

Jennifer A. Noble, Ernesto Marceca, Claude Dedonder, Witchaya Phasayavan, Burapat Inceesungvorn, Geraldine Féraud, Christophe Jouvet

Influence of the N atom position on the excited state photodynamics of protonated azaindole.

Jennifer A. Noble[1*], Ernesto Marceca[2], Claude Dedonder[1], Witchaya Phasayavan[3,4], Geraldine Féraud[1%], Burapat Inceesungvorn[4] & Christophe Jouvet[1]

1 *CNRS, Aix Marseille Univ., PIIM, Physique des Interactions Ioniques et Moléculaires, UMR 7345, 13397, Marseille, France.* jennifer.noble@univ-amu.fr

2 *INQUIMAE (CONICET – Universidad de Buenos Aires), DQIAQF (Facultad de Ciencias Exactas y Naturales, Universidad de Buenos Aires, Ciudad Universitaria), 3er piso, Pab. II, 1428 Buenos Aires, Argentina.*

3 *Graduate School, Chiang Mai University, Chiang Mai 50200, Thailand.*

4 *Department of Chemistry, Center of Excellence in Materials Science and Technology, Chiang Mai University, Chiang Mai 50200, Thailand.*

%Present address: Sorbonne Université, Observatoire de Paris, Université PSL, CNRS, LERMA, F-75005, Paris, France.

Abstract

We present a study of the photofragmentation of three protonated azaindole molecules – 7-azaindole, 6-azaindole, and 5-azaindole – consisting of fused pyrrole-pyridine bicyclic aromatic systems, in which the pyridinic (protonated) nitrogen heteroatom is located at the 7, 6, and 5 positions, respectively. Photofragmentation electronic spectra of the isolated aforementioned azaindolinium cations reveal that their photodynamics extends over timescales covering nine orders of magnitude and provide evidence about the resultant fragmentation pathways. Moreover, we show how the position of the heteroatom in the aromatic skeleton influences the excited state energetics, fragmentation pathways, and fragmentation timescales. Computed ab initio adiabatic transition energies are used to assist the assignation of the spectra, while geometry optimisation in the excited electronic states as well as ab initio calculations along the potential surfaces demonstrate the role of $\pi\pi*/\pi\sigma*$ coupling and/or large geometry changes in the dynamics of these species. Evidence supporting the formation of Dewar valence isomers as intermediates involved in sub-picosecond relaxation processes is discussed.

1. Introduction

The heterocycle *n*-azaindole ($C_7H_6N_2$, also referred to as pyrollopyridine) consists of a substituted indole molecule where a CH moiety on the six-membered ring is replaced by a nitrogen atom. Such aromatic pyrrole-pyridine bicyclic systems, with two nitrogen heteroatoms (one pyrrolic N atom at position 1 and one pyridinic N atom at position *n*), exhibit very interesting chemistry[1] and, because of their similarity with indole, are also of great interest in biochemistry; e.g. the promising application of azaindole derivatives as fluorescent probes in *in-vivo* imaging studies along with being isosteric analogues for tryptophan in proteins.[2]

There has been little to no study of the photophysical properties of most *n*-azaindole molecules, although fluorescence spectroscopic studies on 5-, 6- and 7-azaindole in solution have been carried out.[3-5] In the gas phase, only the 7-azaindole molecule has been extensively studied, with much of the interest in the literature focused on its hydrogen/proton transfer dynamics in the dimer. A

particular interest concerns the investigation of the (N_1H,N_n) ⇌ (N_1,N_nH) tautomerisation mechanism in the excited-state (i.e. H transfer from N_1 to N_n), which was characterised through computational and experimental approaches involving a double proton exchange reaction in azaindole dimers or the formation of cyclic intermediates of azaindole with solvent molecules. The question of whether a stepwise or a concerted mechanism is involved in this excited state multi-proton transfer (ESPT) process remains as yet unresolved.[6-8] To date, little is known about the intermediates participating in this charge transfer process, i.e. protonated/deprotonated or hydrogenated/dehydrogenated forms of 7-azaindole, nor how the efficiency of this mechanism depends on the azaindole *n*-isomer being excited.

Detailed spectroscopic investigations performed directly on isolated molecular cations, e.g. protonated N-bearing aromatic molecules, will shine light on how the charge state affects the photophysical properties of the chromophore, as well as how they can be tuned as a function of the N-atom position in the aromatic skeleton (or side chain), which in turn will normally define the protonation site. In this study we investigate how the skeletal position of the N-atom in protonated 5-, 6-, and 7-azaindole (hereafter denoted as *n*-AIH$^+$) affect their excited state energetics, fragmentation pathways, and fragmentation timescales.

2. Experimental and theoretical methods

The electronic spectra of protonated 5-, 6-, and 7-azaindole ($C_7N_2H_7^+$, sourced from Sigma-Aldrich) were obtained via ion photo-fragmentation spectroscopy in a cryogenically-cooled Paul trap. The set-up has been extensively described elsewhere[9,10] and is similar to those developed in various research groups[11-16] based on the original concept of Wang and Wang.[11,17-19] Protonated ions are produced in an electrospray source,[20] and once extracted from an initial octopole trap are guided towards the Paul trap with electrostatic lenses and deviation plates and decelerated to 5 eV before entering the trap. Under these conditions we do not observe collision-induced dissociation (CID) fragmentation of protonated *n*-azaindole. The ions are trapped for several tens of ms, and during this period they are thermalised to a temperature of around 50 K through collisions with cold helium buffer gas,[21] which is constantly removed by pumping.

Photodissociation of the trapped ions is accomplished with a tuneable OPO laser (EKSPLA), which has a 10 Hz repetition rate, 10 ns pulse width, a spectral resolution of ~ 10 cm^{-1} and a minimum scanning step of 0.02 nm in the range 225– 700 nm. The laser is shaped to a 1 mm^2 spot to fit the entrance hole of the trap and the laser power is around 2 mJ/pulse in the UV spectral region. The precursor and photofragment product ions are extracted after each laser shot. The precursor and product ions are separated in a 1.5 m time-of-flight mass spectrometer and detected using a microchannel plates (MCP) detector. The UV-visible photofragmentation spectra are recorded by detecting simultaneously all the ion signals as a function of the excitation energy.

The laser interacts only once with the ion cloud, the signal is typically averaged over eight shots at each wavelength and the spectra are recorded up to ten times and then averaged (although occasionally, signal intensity and source stability allow us to perform shorter averages). No smoothing procedure was used and noise is due either to statistical uncertainty, instability of the source, or minor fluctuations in the laser power (which were not corrected for).

Multiphoton ionisation (MPI) experiments on neutral n-azaindole molecules were performed in a molecular beam intersected orthogonally by the ionisation laser beam, emitted from the same OPO

system. The experimental setup combines a standard pulsed supersonic expansion with a time of flight mass spectrometer, and has been described in detail in previous publications.[22,23]

Ab initio calculations were performed with the TURBOMOLE (V6.6) package,[24] making use of the resolution-of-the-identity (RI) approximation for the evaluation of the electron-repulsion integrals.[25-27] The equilibrium geometry of ground state (S_0) species were determined at the MP2 (second order Møller−Plesset perturbation theory) and DFT/B3-LYP (density functional theory using the B3-LYP hybrid functional) levels. Zero point energy (ZPE) corrected adiabatic excitation energies of the lowest excited singlet states were determined at the RI-CC2 (second-order approximate coupled-cluster) and TD-DFT (time-dependent density functional theory) levels. Calculations were performed with the correlation-consistent polarized valence double-zeta (cc-pVDZ and aug-cc-pVDZ for $\pi\sigma^*$ states) basis set.[28] Ground and excited state vibrations were calculated, and the electronic spectrum was simulated using PGOPHER software[29] for Franck-Condon analysis.

3. Results and discussion

3.1 *Electronic spectra of protonated 7-, 6-, and 5-azaindole*

The photofragmentation spectra of 7-AIH$^+$, 6-AIH$^+$, and 5-AIH$^+$ are presented in Figure 1. For each of the three species we show the major photofragments, m/z 118 (green trace), m/z 92 (blue trace), and m/z 65 (red trace). Transitions to three electronic excited states are identified from the analysis of the spectra and based on the calculated adiabatic excited state energies. The first fragment (m/z 118) can be attributed to H-loss with formation of the radical cation *n*-AI$^+$, and is present in all electronic excited state transitions of all three species. The second fragment (m/z 92) corresponds to loss of HCN (or HNC), which is a common fragmentation path in nitrogen-containing aromatic compounds, protonated or not (see, for example, the NIST Chemistry Webbook, Pino et al.,[30] or Feraud et al.[31]). This m/z 92 fragment is compatible with $C_6H_6N^+$, which is most likely attributable to ring opening and the formation of a 7-membered ring-expanded heterocyclic structure called an azepinium ion. This aromatic nitrenium ion is isoelectronic to its hydrocarbon analogue, the cycloheptatriene cation ($C_7H_6^+$, normally referred to as tropylium, and frequently observed upon fragmentation of benzyl compounds and many alkylbenzenes such as toluene).[32,33]Although theoretical computations have concluded that azepinium ions should be stable aromatic ions,[34,35] evidence about their formation is limited to mass spectrometric studies concerning the fragmentation of anilines and N-containing heterocycles,[36-38] and a recent synthetic approach of an azepinium ion characterised by NMR spectroscopy. The m/z 92 fragment is weakly observed in the 230-340 nm spectral region for all three species, but gives a particularly strong signal in the electronic excited state lying in the deep UV region, near 225 nm, for 7-AIH$^+$ and 6-AIH$^+$. It should be noted that in this high energy range the loss of H_2 (m/z 117) also becomes a very intense fragment. Such a high energy transition is not observed for 5-AIH$^+$, which is interpreted as a blue shift of the equivalent state for this species to energies beyond our laser range. The third fragment (m/z 65) is common to all three species, and displays approximately the same intensity in each state. However, it is around an order of magnitude lower in intensity than m/z 92 in the high energy transition for 7-AIH$^+$ and 6-AIH$^+$. This fragment may correspond to loss of $C_2H_2N_2$ (or two HCN moieties) and formation of the cation of the five-membered ring cyclopentodienyl, $C_5H_5^+$. Another possibility is formation of the $C_4H_3N^+$ cation, with loss of C_3H_4N (possibly the cyanoethyl radical).

The time of flight photofragmentation mass spectra for protonated 7-, 6-, and 5-azaindole are presented in Figure SI-1 upon excitation in the first and third electronic excited states, together with the spectra obtained by CID fragmentation in the ground electronic state, for comparison. It is worth mentioning that, contrary to the electrospray mass spectra of protonated azaindole molecules

measured in this work by photofragmentation, the CID spectrum is dominated by the m/z 92 fragment, does not include the m/z 118 fragment, and the m/z 65 fragment is weak. It should also be mentioned that the electron impact fragmentation of the 7-azaindole radical cation (m/z 118) yields mainly the m/z 91 fragment (loss of HCN) and, with less intensity, m/z 117 (H loss), m/z 64 and m/z 63 (NIST Chemistry webbook).

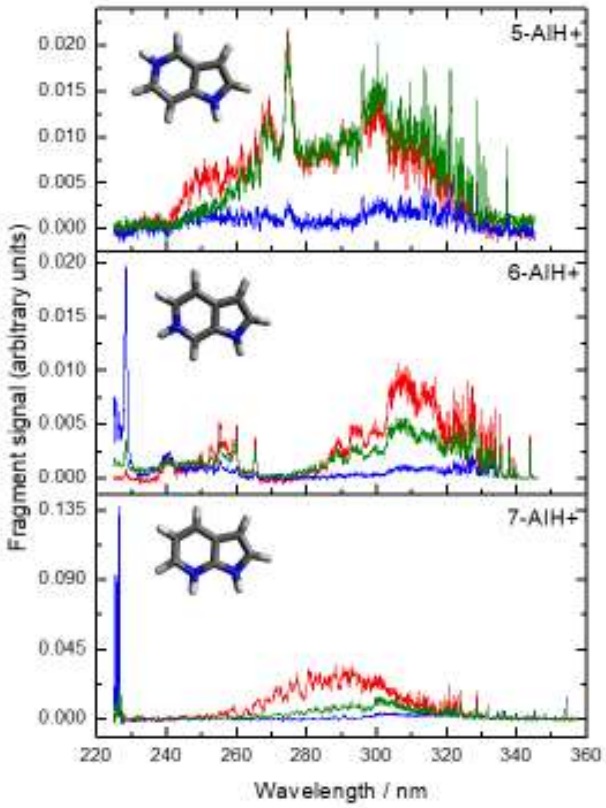

Figure 1: Photofragmentation spectra of protonated 7-, 6- and 5-azaindole measured between 225 and 355 nm. For each species, the fragment traces are as follows: m/z 118 green; m/z 92 blue; m/z 65 red.

The attribution of the experimentally measured excited states is made by comparison to calculations. Experimental and calculated energies of observed electronic excited states (indicated as S_1, S_2, and S_3) are presented in Table 1. The experimentally-derived energy of the 0-0 transition for the S_1 state is similar for all three species, increasing from 3.50 eV for 7-AIH$^+$ to 3.61 eV for 6-AIH$^+$ and to 3.68 eV for 5-AIH$^+$. Based on calculations, and as expected, we can conclude that all three molecules are protonated preferentially on the basic N atom in the six-membered ring (i.e. N_5, N_6, or N_7). The optimised ground state geometries of the most stable protonated azaindole molecules are presented in the ESI (Figure SI-2 and associated text). Protonation on C atoms was found to be around 1.5 eV higher in energy.

In the case of 6-AIH$^+$, the observed S_1 and S_2 states agree well with absorbance data from experiments performed in solutions at low pH, where bands with onsets at ~350 nm (peaking at ~320 nm) and at ~275 nm were attributed to 6-azaindole protonated on the N_6 atom.[4] In the same study, neutral 6-azaindole was observed to absorb from ~320 nm, peaking at ~290 nm. For 5-AIH$^+$, the absorbance peaks in solution at pH 2 were measured at 270 and 291 nm, which also agrees well with

the gas phase spectra in Figure 1, while the neutral absorbance band was observed to peak at 264 nm.[39] The energy of the S_1 state of 7-AIH$^+$ is 0.05 eV higher than that measured by us for the most stable isomer of protonated indole ($C_8NH_8^+$, 3.54 eV for protonation on C_3 in the five-membered ring).[10] In the case of indole, protonation on the C_5, C_6, and C_7 atoms (directly analogous to the position of the N atom in the azaindole isomers) was approximately 0.5 eV less favourable than protonation on C_3. However, the $S_1 \leftarrow S_0$ transitions of these species were calculated to be significantly lower than those of the azaindole molecules (or indeed the C_3 protonated isomer of indole), at 2.75, 2.83, and 2.31 eV for the C_5, C_6, and C_7 protonated isomers of indole, respectively.

State	7-azaindoleH$^+$			6-azaindoleH$^+$			5-azaindoleH$^+$		
	Expt.	Calculated		Expt.	Calculated		Expt.	Calculated	
		DFT	CC2		DFT	CC2		DFT	CC2
S_1	3.50 354nm	3.32 (0.03)	3.53	3.61 343nm	3.74 (0.08)	3.57	3.68 337nm	3.56 (0.03)	3.74
S_2	*4.41[a]* *281nm*	4.56 (0.09)	4.37	4.67 266nm	4.89 (0.01)	4.94	4.51 275nm	4.89 (0.04)	4.66
S_3	5.47 227nm	5.67 (0.40)	5.65	5.43 228nm	5.58 (0.29)	5.58	-	6.03 (0.13)	5.70
πσ* (vertical)			6.16			6.40			6.36

Table 1: Observed excited state energies and calculated adiabatic energies (eV) of protonated 7-, 6-, and 5-azaindole. For DFT calculations, the oscillator strength is given in brackets. [a]Estimated value of the S_2 energy of 7-AIH$^+$ based on the intensity drop observed in the m/z 65 channel and on the calculated value; the assignation is obscured by overlap with the first absorption band.

3.2 Vibrational spectra of the first excited state of protonated 7-, 6-, and 5-azaindole

In all three protonated species, excitation to the S_1 state presents a series of well-defined bands characteristic of a minimal geometry change between the ground and excited states. The vibrational spectra of this state were simulated for each of the species and are presented in Figure 2 alongside the experimental spectra. In all three molecules, the strongest bands in the low energy region of the experimental vibrational spectra are well reproduced by the simulation, although the correspondence becomes poorer at higher energies due to limitations in the simulation method. Experimental and calculated vibrational frequencies are tabulated in Table 2 and a full list of calculated vibrations is given in Table SI-1.

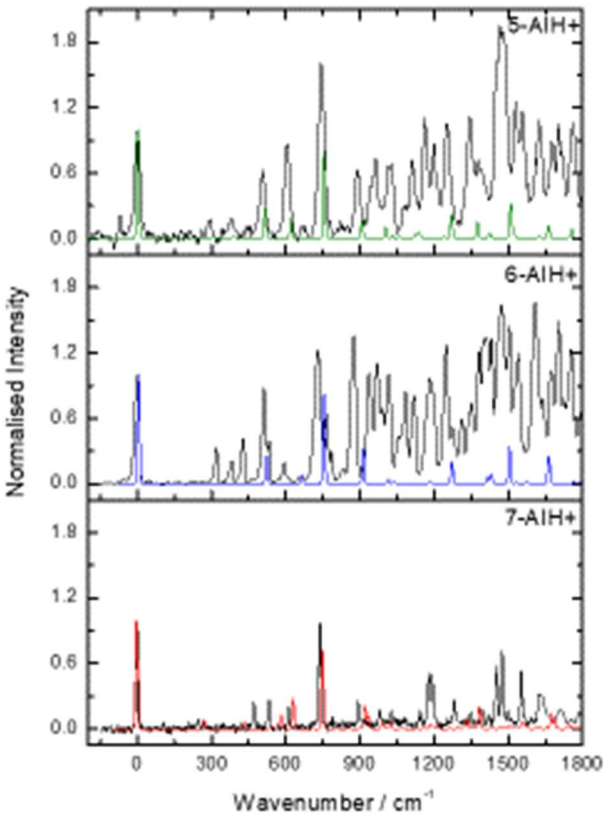

Figure 2: Vibrational spectra of protonated 7-, 6- , and 5-azaindole in the S_1 electronic excited state. For each species, the measured spectrum is in black and the simulated spectrum is in colour (5-AIH$^+$ green, 6-AIH$^+$ blue, 7-AIH$^+$ red).

The vibrational spectra of all three species are relatively similar, with the same modes being populated. For example, the strong band at ~730-745 cm^{-1} for each isomer corresponds to the same in-plane ring breathing mode. The lowest vibrational frequencies (less than 300 cm^{-1}) in S_1 are butterfly modes not present in the experimental spectra, thus one can deduce that the aromatic skeleton stays planar in the excited state. The calculations indicate planar geometries for the 5-AIH$^+$ and the 6-AIH$^+$ ground and excited states, but it should be noted that the excited state geometry calculated for 7-AIH$^+$ is not planar, giving rise to out-of-plane modes such as a very strong band ν_9 at 619 cm^{-1} in the initial simulation. This band is not seen in the experimental spectrum, which clearly means that the calculations are amplifying the out-of-plane character of the S_1 states. Subsequently, the simulation was rerun, suppressing the band, and generating the spectrum presented in Figure 2. A comparison of the spectra produced by both simulations is presented in Figure SI-3. We can conclude that the geometry of the S_1 state is only slightly different to that of S_0 for all isomers. All the calculated frequencies and their symmetries are given in Table SI-1 for the three protonated azaindole molecules.

Table 2: Experimental and calculated vibrational frequencies in S_1 of 5-AIH$^+$, 6-AIH$^+$, and 7AIH$^+$ up to ~1000 cm^{-1}, with vibrational modes attributed where applicable. Tentative attributions are marked with an asterisk. All values are in cm^{-1}

5-azaindoleH$^+$			6-azaindoleH$^+$			7-azaindoleH$^+$		
Expt	Calc	Mode	Expt	Calc	Mode	Expt	Calc	Mode
29660	0	0-0	29078	0	0-0	28233	0	0-0
+291	306	$2\nu_1$	+320	372	$2\nu_1$	+245	273	ν_2
+378	374	$\nu_{1+}\nu_2$	+379	454	$\nu_1+\nu_2$?	+469	438*	ν_4
+443	442	$2\,\nu_2$	+427	393	ν_5	+530	574*	ν_7
+505	514	ν_7	+511	517	ν_6		587*	ν_8
+603	619	ν_{11}	+595	619	ν_9	+615	621	ν_9
+669	676	$2\nu_3$	+659	662	$2\nu_3$	+737	753	ν_{12}
+744	754	ν_{14}	+728	750	ν_{13}	+892	926*	ν_{17}
+821	819	$2\nu_1+\nu_7$	+765	-		+980	995*	ν_{19}
+888	902	$\nu_5+\nu_7$	+783	-				
+963	1002*	ν_{20}	+833	-		+1172		$\nu_4+\nu_{12}$/ $\nu_2+\nu_{17}$
+1023	1028*	$2\nu_7$	+873	909*	ν_{18}	+1196		$\nu_7+\nu_9$
			+941	-				
			+970	1010*	ν_{20}			
			+1017	1034*	$2\nu_6$			

3.3 Fragmentation channel energies

The calculated energies of some fragmentation channels are given in Table 3. We have focused our calculations on the most intense fragments observed (m/z 65, 92, 117, and 118). All possible isomeric forms of the fragments have not been investigated and the barriers or transition states have not been calculated, but conclusions can nonetheless be obtained from these energy values, as detailed in the following paragraphs.

The channel corresponding to H loss (m/z 118) from the N_n (n=7,6,5) atom requires less energy than from the N_1 atom and is energetically possible above 4.77, 4.70, and 4.31 eV for 5-, 6- , and 7-AIH$^+$, respectively (i.e. for wavelengths below 250 nm). In our experiments, this fragment is also observed at wavelengths above 250 nm, implying that H loss in S_1 requires a two-photon absorption.

The formation of the azepinium ion (m/z 92) with loss of HCN is the lowest energy fragmentation channel and can be obtained above 3.65, 3.75, and 3.55 eV for 5-, 6-, and 7-AIH$^+$, respectively, which is close to the experimental origin of the S_1 states, but there is probably a barrier to access that channel. However, in view of the high intensity of this channel in S_3, it seems possible to access to this channel with one photon in S_3.

The formation of $C_5H_5^+$ (m/z 65) with loss of two neutral HCN molecules requires two photon absorption for all excited states. It should be noted that the formation of the m/z 65 fragment could also be a secondary fragmentation i.e. loss of HCN from the m/z 92 fragment.

The H_2 loss channel (m/z 117) has been investigated in the case of loss of the two H atoms attached to the nitrogen atoms. This channel is energetically possible for excitation energies above 5.35 eV for 7-AIH$^+$ and 5.19 eV for 6-AIH$^+$ (i.e. this channel is energetically open when S_3 is excited) but requires some rearrangement of the dehydrogenated positive ion.

Table 3: Fragmentation energies calculated at the DFT/B3-LYP/cc-pVDZ level, relative to the ground state of 7-AIH⁺. [a]Loss of HCN with formation of an azepinium ion is less energetic than other isomers of $C_6H_6N^+$ such as 4-pyridinylmethyl. [b]Loss of the two hydrogen atoms linked to the nitrogen atoms and rearrangement leading to a nine membered ring when the central bond breaks. [c]Loss of two HCN molecules is more favourable than loss of $C_2H_2N_2$.

	Fragmentation energies (eV)					
	Ground/7-AIH⁺	(118^+)/ H-loss from N_n	(118^+)/ H-loss from N_1	(92^+) azepinium + HCN[a]	(117^+)/ loss of H_2	(65^+)$C_5H_5^+$ +2 HCN[c]
7-AIH⁺	0.00	4.31	4.40	3.55	5.35[b]	6.55
6-AIH⁺	-0.22	4.7	5.78	3.75	5.19	6.77
5-AIH⁺	-0.01	4.77	5.77	3.65	4.90	6.65

3.4 Relaxation dynamics in the excited states

In the fragmentation process, one can distinguish between the early (ultrafast) step which concerns the decay of the excited state and the long term dynamics occurring mainly on the ground state surface after internal conversion. In this section, we comparatively discuss the distinct lifetimes of the excited states S_2 and S_3 for 5-, 6- and 7-AIH⁺, addressing the analysis of the long-term dynamics in section 3.5. Lifetimes were estimated exclusively from the observed bandwidths, assuming that coupling to other states hardly contributes to the relaxation process.

A remarkable result concerns the S_3 state in 6-AIH⁺ and 7-AIH⁺, which exhibits a fast and peculiar relaxation process, as deduced from the photofragmentation spectra presented in Figure 3. The major fragment is m/z 92, while m/z 118 and 65 are very weak. The fragment m/z 117 – corresponding to the loss of H_2 – is observed at relatively high abundance, particularly in the S_3 state of 6-AIH⁺ (violet, Figure 3).

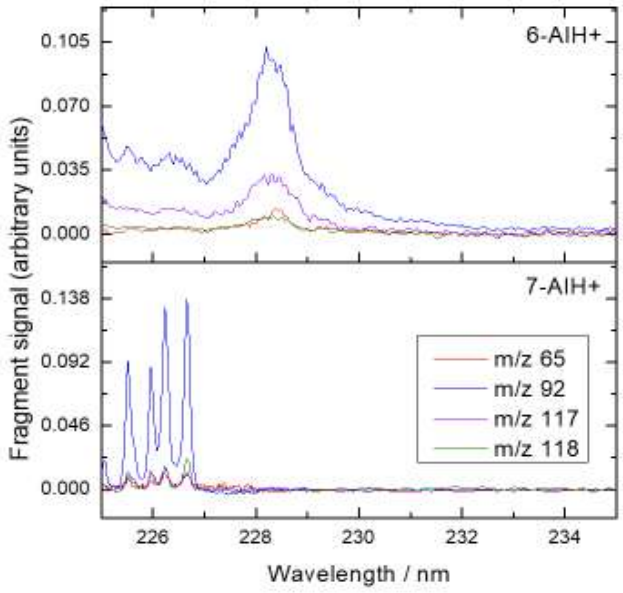

Figure 3 Fragmentation patterns in S_3 for 7-AIH⁺ and 6-AIH⁺. For each species, the fragment traces are as follows: m/z 118 green; m/z 117 violet; m/z 92 blue; m/z 65 red.

Not only is fragment m/z 92 the most intense signal in the S_3 spectrum, but the fragmentation yield in this state is much higher than in S_2 and S_1. Fragmentation which is selective depending upon the excitation energy has previously been observed in aromatic amino ions (aromatic amino acids[40] or aromatic amines[41]), but in those cases the selective effect was clearly attributable to the excitation of the electron into an orbital located on the amino group, leading to subsequent H-loss or proton transfer. In this case, however, *n*-AIH$^+$ has no functional groups (amine, carbonyl) attached to the aromatic skeleton.

3.4.1 Ultrafast dynamics in 7-AIH$^+$

Taking 7-AIH$^+$ as an example, we can identify other characteristics of the S_3 state which distinguish it from S_1 and S_2, namely it has a high calculated oscillator strength (f=0.4) which is around an order of magnitude higher than those of S_1 (f=0.03) and S_2 (f=0.09). This is in agreement with the much stronger fragmentation signal in S_3 than in S_1. Additionally, the absorption cross section inferred from the power dependence of the photofragmentation signal (presented in Figure SI-4) is a factor of ten higher for S_3. This state also presents low vibrational frequencies (~70 cm^{-1}) compared to the ground state and S_1, as can be seen in Figure SI-5.

The S_3 state also displays significantly faster excited state relaxation dynamics than S_1, as inferred from the widths of the vibronic bands. As can be observed in the lower panel of Figure 2, the width of all vibrational bands in the S_1 state of 7-AIH$^+$ is ~10 cm^{-1}, which corresponds to the spectral width of the laser. However, the same species has vibrational bands with a width of 23 cm^{-1} in the S_3 (derived by fitting Lorentzian peaks to the experimental data, as illustrated in Figure SI-5). Broad bands in the experimental electronic spectrum can reveal the presence of short excited state lifetimes, as has already been observed for other protonated systems, such as the protonated DNA bases[42] or aromatic amines.[41] The bandwidths in the S_3 state of 7-AIH$^+$ can be attributed to lifetime broadening, with a derived lifetime of ~230 fs.

The aforementioned spectroscopic pattern and dynamics of 7-AIH$^+$ in the S_3 state can be explained by the presence of a conical intersection (CI), in the form of a $\pi\pi^*/\pi\sigma^*$ crossing, as has been demonstrated repeatedly for N-bearing aromatic molecules, both neutral and protonated.[43] The first evidence supporting the existence of the CI comes from the presence of low frequency vibrational modes in S_3. To be so low, these vibrations must be out-of-plane modes, meaning that the planar geometry of 7-AIH$^+$ is distorted upon excitation to the deep-UV S_3 state. This is a clear indication of strong interaction of the S_3 state with another close lying state, which we will identify in the forthcoming paragraphs as the $\pi\sigma^*$ state.

Further evidence for the presence of a $\pi\pi^*/\pi\sigma^*$ crossing comes from the calculations performed in Cs symmetry at the CC2/aug-cc-pVDZ level. We found that the third excited state of A'($\pi\pi^*$) symmetry (S_3) has a strong oscillator strength associated with a vertical excitation energy of 5.94 eV (corresponding to an adiabatic energy of 5.67 eV/219 nm, see Table 1). On the other hand, the first A" state has a strong $\pi\sigma^*$ character with a diffuse orbital on the plane localised on the hydrogen atoms attached to both N_7 and N_1. This state corresponds to a vertical energy of 6.16 eV and is nearly dissociative upon excited state optimisation, increasing the N_7-H bond, as illustrated in Figure 4 (left hand panel). The $\pi\sigma^*$ state crosses the 3A' (S_3 $\pi\pi^*$) at around 5.85±0.05 eV, i.e. 0.3 eV above the minimum energy of the $\pi\pi^*$ S_3 state. At first glance, this seems to be a typical example of the $\pi\pi^*/\pi\sigma^*$coupling model (SDDJ model)[44] where the excited state dynamics is controlled by the H-loss and the $\pi\pi^*/\pi\sigma^*$ coupling. However, in this case the H-loss process is not strongly observed upon the excitation of this 3A' state, although this channel is energetically open. Optimisation of the $\pi\sigma^*$ state leads to a stable form at 4.67 eV, presented in Figure 4, in which the N_7..H bond is elongated to 2.5 Å

and which is the ground state of the system at this geometry, implying that the $\pi\sigma^*$ state crosses S_3, S_2, S_1 and S_0.

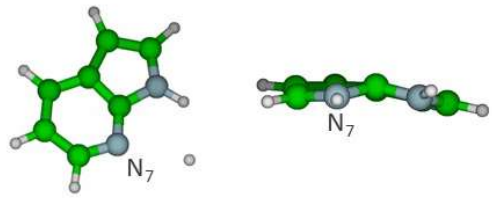

Figure 4: Left panel: optimised geometry of the 1A" ($\pi\sigma^*$) state of 7-AIH$^+$, resulting in quasi NH dissociation. Right panel: optimised geometry of the S_3 ($\pi\pi^*$) state, resulting in a distorted plane.

The $\pi\pi^*/\pi\sigma^*$ coupling can also be discerned in the optimisation of the S_3 state when releasing the Cs symmetry in the calculation, which leads to a deformation of the indole plane (right hand panel of Figure 4). The resulting two lowest calculated vibrational modes are at 103 and 160 cm^{-1}, i.e. a lot smaller than those calculated for S_1 (Figure 2) and in good agreement with the observed experimental bands (70 cm^{-1}), illustrating the effect of the $\pi\pi^*/\pi\sigma^*$ coupling.

3.4.2 Ultrafast dynamics in 6-AIH$^+$ and 5-AIH$^+$

The S_2 state is only clearly visible in the experimental spectra of 6-AIH$^+$ and 5-AIH$^+$, where it exhibits approximately the same fragmentation patterns as in S_1. In the S_2 state, both 5-AIH$^+$ and 6-AIH$^+$ exhibit lifetime broadening effects, unlike the S_1 state where the observed linewidths are as small as 10 cm^{-1} and entirely attributable to the spectral width of the laser. In 5-AIH$^+$, the 0-0 transition of S_2 is rather wide, i.e. it exhibits a measured bandwidth of ~280 cm^{-1}, corresponding to a lifetime of ~20 fs. Likewise, in 6-AIH$^+$, the 0-0 transition of S_2 exhibits a measured bandwidth of ~115 cm^{-1} that corresponds to a lifetime of ~50 fs.

The bands of the S_3 state of 6-AIH$^+$ are significantly more broadened than those of 7-AIH$^+$, with a bandwidth of 230 cm^{-1} corresponding to a lifetime of only ~25 fs. Furthermore, upon comparison of the 0-0 transitions of S_1, S_2, and S_3 for 6-AIH$^+$, presented in Figure 5, it is clear that S_2 and S_3 have progressively shorter lifetimes than S_1. Since the S_3 state of 5-AIH$^+$ was not probed within the laser wavelength range employed in the experiment, the following discussion will be limited to a comparison between the excited state dynamics of 7-AIH$^+$ and 6-AIH$^+$. It is clear from observation of Figure 5, that the three excited states of 6-AIH$^+$ display similar vibrational structure, indicating that a fast, non-radiative decay takes place in S_2 and S_3. However, for 6-AIH$^+$, the combination of a very fast lifetime without deformation of the excited state potential in the Franck Condon region (the S_3 state stays planar) may not be due to the $\pi\pi^*/\pi\sigma^*$ interaction, as was the case of 7-AIH$^+$, because the energy gap is greater, the $\pi\sigma^*$ state of 6-AIH$^+$ being calculated 0.5 eV higher than that in 7-AIH$^+$.

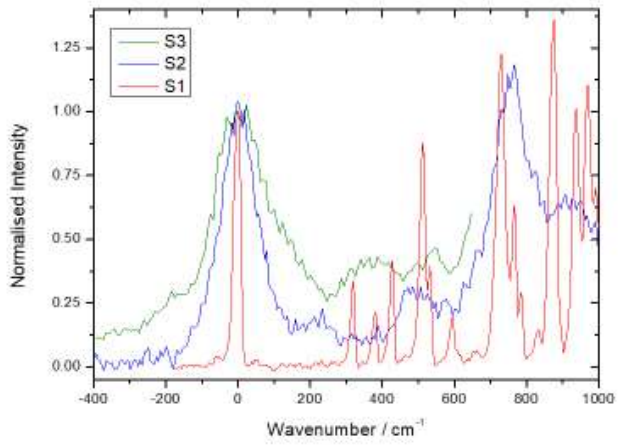

Figure 5: Excited states S_1, S_2, and S_3 of 6-AIH$^+$. The lifetimes of the states are approximately 50 fs (S_2) and 25 fs (S_3).

Some clues for another explanation for the short lifetime of the S_3 state in 6-AIH$^+$ may be extracted by comparison with observations in other similar molecules. It should first be noted that the gas phase spectra of neutral 5-azaindole and 6-azaindole have not been reported in the literature through MPI or through fluorescence excitation, and that our attempts to measure these spectra by MPI were unsuccessful while, under the same experimental conditions, the 7-azaindole gave a strong spectral signal (Figure SI-6). We attribute the non-detection of 5-azaindole and 6-azaindole precisely to their very short lifetimes which prevent the absorption of multiple photons.[1]

3.4.3 *Comparison with other systems*

Similar lifetime variation according to the position of the nitrogen atom in the ring has been observed in protonated quinoline and isoquinoline. These molecules are analogous to 7-AIH$^+$ and 6-AIH$^+$, respectively, but with the five-membered ring replaced by a six-membered hydrocarbon aromatic ring (i.e. benzene). In the case of protonated isoquinoline (equiv. to 6-AIH$^+$), the excited state lifetime of the S_3 state is very short, while for quinoline (equiv. to 7-AIH$^+$), the lifetime is around four times slower.[31,45] Taking into consideration the observations above, it seems reasonable to deduce that when a nitrogen atom occupies the 5- or 6- positions in the six-membered ring, the excited state lifetime is shorter.

A possible explanation can be derived from a comparison with the excited state relaxation of both pyridine- and pyrimidine-type molecules via the formation of the Dewar structure in the six-membered ring, which has previously been observed and calculated.[46-48] Two types of structures can be obtained for a single, N-bearing six-membered ring: one results in the formation of a central C-C bond, while the other in forming a central C-N bond. In neutral pyridine, the transition state energy to form the C-C Dewar structure is 3.7 eV, somewhat smaller than the 4.6 eV required for the C-N Dewar type.[49] Moreover, the $S_0 \leftarrow S_1$ conical intersection leading to the Dewar structure is endothermic for the formation of the C-N Dewar type, but exothermic for the C-C type.[49] Thus, it

[1] During the revision period for this manuscript, Lamas et al.[52] published a fs time-resolved ionisation study of neutral 4-, 5-, 6- and 7-azaindole in which they confirm ultrashort lifetimes for 5- and 6-azaindole

turns out that the C-C type Dewar structure of pyridine, besides being energetically more stable, also has no kinetic barrier to its formation from the excited state.

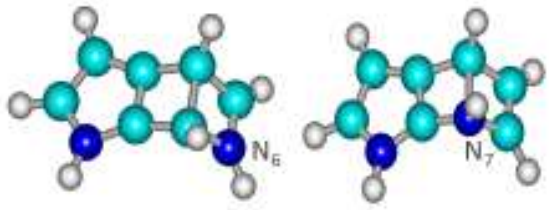

Figure 6: Optimised geometries of (left) C-C 6-AIH⁺ and (right) C-N 7-AIH⁺ Dewar structures.

In the case of the bicyclic azaindole molecule, geometry constraints restrict 7-azaindole to forming exclusively the C-N type of Dewar structure, and 6- or 5-azaindole to forming only the C-C type Dewar. Calculated Dewar structures for 6-AIH$^+$ and 7-AIH$^+$ (see Figure 6) have energies of 4.3 eV above S_0 for the 6-AIH$^+$ C-C Dewar type and 4.8 eV above S_0 for the 7-AIH$^+$ C-N Dewar type, implying that the C-C Dewar structure is energetically more accessible. Similarly, we have found that the energies of the Dewar structures for protonated isoquinoline and quinoline are 3.4 eV and 3.9 eV, respectively, again favouring the formation of C-C Dewar intermediates. A simple schematic of the reaction pathway derived from the theoretical work of Su[49] is given in Figure SI-7.

This discussion about Dewar structures – while having the merit of reconciling observed behaviour in a number of similar systems – is somewhat speculative at this time and we are preparing a series of experimental and theoretical tests to further probe this explanation. In particular, we would like to explore the transition states and the barriers to the formation of Dewar structures in N-bearing multiple ring aromatics.

3.5 Fragmentation dynamics and mechanisms at longer timescales

The major photofragments are m/z 118 (H loss), m/z 117 (H_2 loss), m/z 92 (azepinium), and m/z 65. To complete the discussion of relaxation pathways, we will now show that the m/z 118 and m/z 92 fragments do not belong to the same fragmentation path by means of delayed ion extraction experiments. The relaxation pathways discussed here are summarised in Figure SI-8.

First we focus on the fragmentation pattern of 7-AIH$^+$ in the S_3 state (presented in Figure 3), but it should be noted that similar observations have been made in 6-AIH$^+$. By varying the time between photoexcitation of the precursor ion and the extraction of ions (precursor and product) from the Paul trap, the fragmentation dynamics along each pathway can be studied at timescales down to the instrumental resolution limit of our instrument, estimated as ~0.5 µs. Figure 7 presents the fragment signal as a function of extraction time for the major fragments m/z 118, m/z 117, m/z 92 and m/z 65 in S_1 and S_3 of 7-AIH$^+$. It is clear that the appearance times of the major fragment m/z 92 as well as fragment m/z 117 in S_3 are very long (~0.3 ms) compared to all other channels, which exhibit dynamics on the order of the µs or shorter (as extracted by fitting exponential and erf (1-exp(-a*t))

functions convolved by a Gaussian representing the instrument response to the experimental data, as plotted in Figure 7). The CID fragmentation pattern of 7-AIH$^+$ also illustrates that the m/z 92 fragment is produced by ground state collision induced fragmentation, but not m/z 118, which is already an indication that m/z 92 can be produced as a primary fragment. Besides, the fragmentation pattern of the radical cation 7-azaindole$^+$ (m/z 118) under low energy electron impact conditions (NIST Chemistry Webbook) shows that m/z 91 is the product fragment of m/z 118). We can thus conclude that the product fragment m/z 118 (i.e. 7-AI$^+$, the radical cation of 7-azaindole) corresponding to the dehydrogenated 7-AIH$^+$ precursor ion does not give rise to m/z 92.

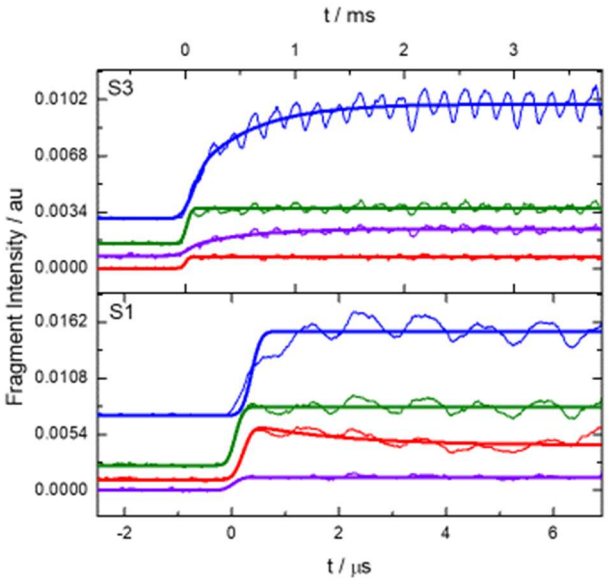

Figure 7: Fragmentation dynamics of 7-AIH$^+$ in S_3 (upper panel, ~4 ms) versus S_1 (lower panel, ~9 µs) for fragments m/z 118 (green), m/z 117 (violet), m/z 92 (blue), and m/z 65 (red). Fits to experimental data are overplotted in thick lines.

Another piece of evidence supporting this conclusion is our experiment performed on the neutral 7-azaindole molecule, a species for which the resonance-enhanced one-colour two-photon ionisation (REMPI) spectrum is well known.[50] In Figure SI-6 we present the REMPI spectrum measured at m/z 118 (7-AI$^+$) in our molecular beam experiment, which corresponds well to previously published spectra. [50] With one-colour multi-photon spectroscopy, we observed a weak signal corresponding to the photofragmentation of 7-AI$^+$, producing the fragment m/z 91 (i.e. the equivalent of the product ion m/z 92 in 7-AIH$^+$) with the laser set at 288.7 nm, the origin peak of S_1. This is further evidence that the product fragment of the radical cation 7-AI$^+$ is m/z 91 and not m/z 92, and thus the fragment m/z 92 in the S_3 of 7-AIH$^+$ is not produced from the m/z 118 radical cation. The above discussion allows us to confirm that the protonated molecule has a distinct dissociation mechanism, producing the fragment m/z 92 via a primary fragmentation.

What plausible mechanisms are compatible with the fragmentation channels observed? To make a long story short, we can understand the fragmentation in the following manner: the fragmentation occurs in the ground state after internal conversion and there are different ways to reach S_0 from the excited state ($\pi\sigma^*$ or Dewar). The resulting ion is very hot, and it fragments following different

channels. In the S_3 state of 7- or 6-AIH$^+$, the very slow processes forming m/z 117 (H_2 loss) and m/z 92 (azepinium ion) with dynamics of ~0.3 ms, are probably due to a high barrier and to a one photon process. Indeed, the S_3 state has an oscillator strength ten times larger than S_1 and S_2, a very short lifetime and the laser power is five times smaller than at lower energy. Thus the energy imparted to the ion is around 5.4 eV – probably slightly above the barriers, implying a slow process. The two slow channels in S_3, H_2 loss or formation of $C_6NH_6^+$ and HCN, cannot be part of a sequential process, i.e. loss of H_2 followed by the formation of $C_6NH_6^+$ and HCN is not possible since there are not enough H atoms in the system.

In CID, m/z 92 is observed but not H_2 loss. This can be understood if the barrier to the H_2 loss channel is higher than the barrier to produce the m/z 92 fragment. For a well-defined energy, the reaction rate is governed by the sum of the H_2 loss rate and m/z 92 rate, while the difference in energy is reflected in the abundance of the fragments (H_2 loss being around five times less intense than formation of m/z 92). On the other hand, the CID process is a gradual and "slow" heating of the ion, in which case the ion fragments as soon as the energy of the lowest barrier is reached and never acquires enough energy to reach the second barrier.

At lower energy, when S_1 and S_2 are excited, the fragments ($C_4NH_3^+$ m/z 65, m/z 118, m/z 92) are obtained within μs. Our power dependence measurement indicates that the absorption is a one-photon process in all the excited states, although we have calculated that energetically the fragmentation process requires two photons. We thus conclude that the lower energy $S_1 \leftarrow S_0$ transition is saturated in our experiments. That is, upon two photon absorption in the S_1 state the energy deposited in the ion is higher than 7 eV, much greater than the energy deposited in the ion upon excitation of the S_3 state, and this leads to fast fragmentations as represented in the lower panels of Figure 7 and the opening of higher energy channels (m/z 65).

The overall conclusion is that the understanding of the full dynamics of 6- and 7-AIH$^+$ requires the observation of the processes over nine orders of magnitude. Dynamics in a range covering 13 orders of magnitude (fs-ms) have already been observed in the case of protonated tryptophan.[20,51] However, in that case the very long time scale processes are due to fragmentation of product ions, in which the internal energy is not well defined. For 6- and 7-AIH$^+$, the long timescale process is, instead, a primary fragmentation process, implying that the transition state is quite high in energy. This is not surprising, given that the transition state energy for the simplest rearrangement from the benzylium to tropylium cation has been calculated at around 3 eV, implying an isomerisation rate on the order of 10^4 s^{-1}.[32]

4. Conclusion

We have presented the electronic spectra of protonated 7-, 6-, and 5-azaindole ions, attributing the experimentally observed bands by reference to calculations. We have shown that the position of the N atom in the ring fundamentally impacts the energy of, and photofragmentation dynamics in, electronically excited states of the molecule. We explain the appearance of short-lived excited states in 7-AIH$^+$ by the presence of $\pi\pi^*/\pi\sigma^*$ coupling, as in the standard SDDJ model. However, for 5-AIH$^+$ and 6-AIH$^+$, we postulate the formation of Dewar structures to explain the excited state lifetimes which are much shorter than in 7-AIH$^+$.

5. Acknowledgements

This work has been conducted within the International Associated Laboratory LEMIR (CNRS/CONICET) and was supported by CONICET, FONCyT, SeCyT-UNC, CNRS (INSIS), and the ANR Research Grant (ANR2010BLANC040501-ESPEM and ANR17CE05000502-Wsplit). WP acknowledges the financial support of Chiang Mai University, Campus France and the PHC SIAM exchange program. The authors acknowledge the use of the computing facility cluster Meso-LUM of the LUMAT federation (LUMAT FR 2764).

Bibliography

[1] Mérour J.Y., and Joseph B., Current Organic Chemistry 2001, 5, 471-506

[2] Merkel L., Hoesl M.G., Albrecht M., Schmidt A., and Budisa N., ChemBioChem 2010, 11, 305-314

[3] Chen Y., Rich R.L., Cai F., and Petrich J.W., J PhysChem 1993, 97, 1770-1780

[4] Twine S.M., Murphy L., Phillips R.S. et al, J PhysChem B 2003, 107, 637-645

[5] Cash M.T., Schriener P.R., and Phillips R.S., Organic and Biomolecular Chemistry 2005, 3, 3701-3706

[6] Catalán J., del Valle J.C., and and Kasha M., Proc. Natl. Acad. Sci. U. S. A. 1999, 96, 8338–8343

[7] Kwon O.H., and Zewail A.H., Proc. Natl. Acad. Sci. U. S. A. 2007, 104, 8703–8708

[8] Crespo-Otero R., Kungwan N., and Barbatti M., Chemical Science 2015, 6, 5762-5767

[9] Noble J. A., Broquier M., Grégoire G., Soorkia S., Pino G., Marceca E., Dedonder-Lardeux C. and Jouvet C., Phys. Chem. Chem. Phys., 2018, 20, 6134-6145

[10] Alata I., Bert J., Broquier M., Dedonder C., Feraud G., Grégoire G., Soorkia S., Marceca E., and Jouvet C. Journal of Physical Chemistry A 2013, 117, 4420-4427

[11] Ishiuchi S., Wako H., Kato D., and Fujii M., J. Mol. Spectrosc. 2017, 332, 45-51

[12] Burke N. L., Redwine J. G., Dean J. C., Mcluckey S. A., and Zwier T. S., Int. J. Mass Spectrom. 2015, 378, 196-205

[13] Inokuchi Y., Haino T., Sekiya R., Morishima F., Dedonder C., Raldine G., Raud F., Jouvet C., and Ebata T., Phys. Chem. Chem. Phys. 2015, 17, 25925-25934

[14] Choi C. M., Choi D. H., Kim N. J., and Heo J., Int. J. Mass Spectrom. 2012, 314, 18-21

[15] Günther A., Nieto P., Müller D., Sheldrick A., Gerlich D., and Dopfer O., J. Mol. Spectrosc. 2017, 332, 8-15

[16] Kamrath M. Z., Relph R. A., Guasco T. L., Leavitt C. M., and Johnson M. A., Int. J. Mass Spectrom. 2010, 300, 91-98

[17] Wang X.-B., and Wang L.-S., Rev. Scien. Inst. 2008, 79, 73108

[18] Wang L.-S., J. Chem. Phys. 2015, 143, 40901

[19] Marsh B. M., Voss J. M., and Garand E. A., J. Chem. Phys. 2015, 143, 204201

[20] Andersen J. U., Cederquist H., Forster J. S., Huber B. A., Hvelplund P., Jensen J., Liu B., Manil B., Maunoury L., Nielsen S. B.; et al., Phys. Chem. Chem. Phys. 2004, 6, 2676-2681

[21] Esteves-López N., Dedonder-Lardeux C., and Jouvet C., J. Chem. Phys. 2015, 143, 74303

[22] Jouvet C., Lardeux-Dedonder C., Richard-Viard M., Solgadi D., and Tramer A., J. Phys. Chem. A 1990, 94, 5041-5048

[23] Huang X., Aranguren J.-P., Ehrmaier J., Noble J.A., Xie W., Sobolewski A.J., Dedonder-Lardeux C., Jouvet C., and Domke W., Phys. Chem. Chem. Phys. 2020, 22, 12502-12514

[24] TURBOMOLE V6-6 2011, a development of University of Karlsruhe and Forschungszentrum Karlsruhe GmbH, 1989-2007, TURBOMOLE GmbH, since 2007; available from http://www.turbomole.com.

[25] Hattig C., J. Chem. Phys.2003, 118, 7751-7761

[26] Hättig C., Phys. Chem. Chem. Phys.2005, 7, 59

[27] Hättig C., and Weigend, F., J. Chem. Phys.2000, 113, 5154

[28] Woon D. E., and Dunning Jr., T. H., J. Chem. Phys.1993, 98, 1358

[29] PGOPHER, a Program for Simulating Rotational Structure, C. M. Western, University of Bristol, Http://pgopher.chm.bris.ac.uk.

[30] Pino G. A., Feraud G., Broquier M., Grégoire G., Soorkia S., Dedonder C., and Jouvet C., Phys. Chem. Chem. Phys., 2016, 18, 20126 -20134

[31] Féraud G., Domenianni L., Marceca E., Dedonder-Lardeux C., and Jouvet C., J. Phys. Chem. A 2017, 121, 2580-2587

[32] Fridgen T. D., Troe J., Viggiano A. A., Midey A. J., Williams S., and McMahon T. B., J. Phys. Chem. A 2004, 108, 5600-5609

[33] Fati D., Lorquet A. J., Locht R., Lorquet J. C., and Leyh B., J. Phys. Chem. A 2004, 108, 9777-9786

[34] Smith D. A., and Bitar J., J. Org. Chem. 1993, 58, 6-8

[35] Di Stefano M., Rosi M., Sgamellotti Q., and Negri F., Chem. Phys. 2004, 302, 295-308

[36] Robertson A.V., and Djerassi C., J. Am. Chem. Soc. 1968, 90, 6992-6996

[37] Marx M., and Djerassi C., J. Am. Chem. Soc. 1968, 90, 678

[38] Wickens J. R., Sleeman R., and Keely B. J., Rapid Commun. Mass Spectrom. 2007, 21, 2491-2496

[39] Mahadevan I., and Rasmussen M., J. Heterocyclic Chem. 1992, 29, 359-367

[40] Féraud G., Broquier M., Dedonder-Lardeux C., Grégoire G., Soorkia S., and Jouvet C., Phys. Chem. Chem. Phys. 2014, 16, 5250-5259

[41] Noble J.A., Dedonder-Lardeux C., Mascetti J., and Jouvet C., Chem. Asian J. 2017, 125, 1523-1531

[42] Berdakin M., Féraud G., Dedonder-Lardeux C., Jouvet C., and Pino G.A., Phys. Chem. Chem. Phys. 2014, 16, 10643-10650

[43] Noble J.A., Dedonder C., and Jouvet C., in “Physical Chemistry of Cold Gas Phase Functional Molecules and Clusters”, edited by T. Ebata and M. Fujii, 2019 Springer, Singapore

[44] Sobolewski A. L., Domcke W., Dedonder-Lardeux C., and Jouvet, C., Phys. Chem. Chem. Phys. 2002, 4, 1093-1100

[45] Hansen C. S., Blanksby S. J., and Trevitt A. J., Phys. Chem. Chem. Phys. 2015, 17, 25882-25890

[46] Kudoh S., Takayanagi M., and Nakata M., J. Photochem. Photobiol. A Chem. 1999, 123, 25-30

[47] Delchev V.B., Sobolewski A.L., and Domcke W., Phys. Chem. Chem. Phys. 2010, 12, 5007-5015

[48] Estevez-Lopez N., and Coussan S., J. Mol. Struc. 2017, 1172 , 65

[49] Su M.-D., J. Phys. Chem. A 2007, 111, 971-975

[50] Huang Y., Arnold S., and Sulkes M., J. Phys. Chem. 1996, 100, 4734-4738

[51] Lepère V., Lucas B., Barat M., Fayeton J.A., and Picard V.J., J. Chem. Phys. 2007, 127, 134313

[52] Lamas I., Montero R., Martinez-Martinez V., Longarte A., and Blancafort L., Phys. Chem. Chem. Phys. 2020, 22, 18639-18645

ToC Entry

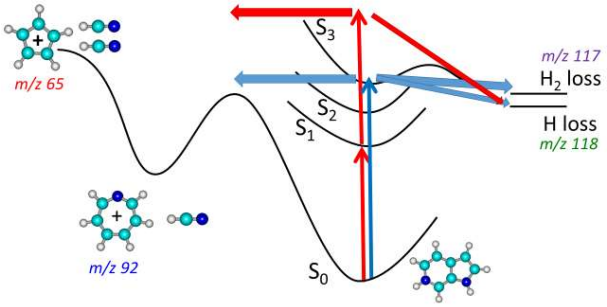

Competition between relaxation pathways from S_1 and S_3 in protonated *n*-azaindole